Journal of ELECTRONIC MATERIALS, Vol. 41, No. 11, 2012
DOI: 10.1007/s11664-012-2233-0
© 2012 TMS

Transient Thermal Impedance Measurements on Low-Temperature-Sintered Nanoscale Silver Joints

YUNHUI MEI,[1] TAO WANG,[2] XIAO CAO,[3] GANG CHEN,[2,4] GUO-QUAN LU,[1,3] and XU CHEN[2]

1.—Tianjin Key Laboratory of Advanced Joining Technology and School of Material Science and Engineering, Tianjin University, Tianjin, People's Republic of China. 2.—School of Chemical Engineering and Technology, Tianjin University, Tianjin, People's Republic of China. 3.—Department of Electrical and Computer Engineering, Virginia Polytechnic Institute and State University, Blacksburg, VA 24061, USA. 4.—e-mail: agang@tju.edu.cn

A measurement system for thermal impedance (Z_{th}) was developed to evaluate the transient thermal performance of sintered nanoscale silver joints. Five different temperature profiles for low-temperature sintering were evaluated by Z_{th} measurements of the joints. The thermal impedance of the sintered samples was altered by the different sintering conditions. Samples that underwent heating profiles with a separate drying stage offered lower thermal impedance than those sintered directly. Exerting pressure of more than 1 MPa during sintering insignificantly improved the thermal impedance. Besides, the impedance could be lowered by extending the holding time of the drying stage and applying pressure as low as 1 MPa during sintering. Characterization of microstructures of the sintered layers was performed by scanning electron microscopy (SEM). With more cracks present, the thermal impedance of the chip joints increased. The presence of cracks was possibly attributed to fast drying or the lack of a drying step.

Key words: Thermal impedance, nanoscale silver, die-attach, silver joints, low-temperature sintering, insulated gate bipolar transistor (IGBT)

INTRODUCTION

Low-temperature joining technology (LTJT) using microscale silver is emerging as a lead-free solution for high-performance, high-reliability, and high-temperature applications.[1–3] LTJT can improve temperature cycling capability by five times and shows five times longer lifetime compared with solder-based attachments, when chip junction temperature goes up to 175°C. However, a serious drawback of LTJT is the necessity to apply a high pressure (>40 MPa) in order to lower the sintering temperature to as low as 300°C. This aspect limits actual production throughput and increases the cost, thus slowing down its adoption. The development of a suitably formulated nanoscale silver paste with particle size of 30 nm,[4–14] which can be sintered at low temperature, i.e., 275°C, without pressure for attaching 3 mm × 3 mm chips could pave the way for widespread implementation of LTJT in electronic manufacturing, starting with high-power-density electronics, e.g., some automotive power electronics, where improved joint performance is desired.

When the paste was used in large-area die-attachment, defects could appear in the silver joint,[15] which increased the thermal impedance of assemblies, and correspondingly the junction temperature of chips. Therefore, the thermal impedance could be chosen as a quality criterion for the nanoscale silver attached device. It is known that SiC devices can work at higher temperature and lower the junction temperature, which is beneficial in terms of device efficiency and lifetime.[16–18] However, based on previous work,[19] microcracks in the

(Received June 25, 2011; accepted August 6, 2012; published online September 8, 2012)

5 mm × 5 mm silver joints still emerged. Interfacial thermal impedance between different components can arise from a combination of poor mechanical and chemical adherence at the interface.[20] Various heating profiles were tested to eliminate these defects.[15] Applying pressure on the joint during processing was also preferred for large-area attachments. The bonding strength of the sintered nanoscale silver joint was reported to be substantially improved by applying pressure.[15] Therefore, the effect of sintering pressure on the thermal impedance also needs to be investigated to enhance the performance of nanoscale silver joints.

However, the thermal impedance of sintered nanoscale silver joints had only been measured by Xiao et al. and Gang et al. until now.[21–23] In Xiao et al.'s work,[21,23] they developed a transient thermal impedance measurement system and studied the influence of thermal cycling (−40°C to 125°C) on different die-attach materials, e.g., nanoscale silver. Then, Gang et al.[22] compared the transient thermal impedance of three common die-attach materials. They disclosed that the transient thermal impedance of sintered nanoscale silver was significantly lower than that of lead-free solders. As a result of the good thermal and electric performance of the sintered nanoscale silver, it therefore becomes necessary to pay more attention to study how to obtain sintered nanoscale silver joints with outstanding thermal performance.

The objective of this study is to compare the thermal impedance of sintered nanoscale silver joints made using different heating profiles and pressures. Since some scholars found that the thermal impedance showed functional dependence on the bonding strength,[24] thermal impedance should be also an important parameter as well as die-shear strength for evaluating the quality of sintered nanoscale silver joints.

EXPERIMENTAL PROCEDURES

Sample Preparation

Samples were prepared as follows: insulated gate bipolar transistor (IGBT) die (International Rectifier: IRG4CH30K), mainly made up of silicon with dimensions of 0.38 mm × 3.5 mm × 5 mm, were connected to silver-coated copper substrates (6 mm × 25 mm × 25 mm) by sintered nanoscale silver. The nanoscale silver paste, obtained from NBE Tech, LLC,[25] was made by adding selected organic surfactant, binder, and thinner to 30-nm nanoscale silver particles as suggested by the manufacturer.[26,27] Then, the mixture solution was agitated ultrasonically to obtain a uniform distribution of nanoscale silver particles. A vacuum evaporation process was applied to remove the organic solvent, and a paste form was obtained. The paste could be readily processed by common surface-mount techniques, such as screen/stencil printing or syringe dispensing. About 0.5 g nanoscale silver paste, controlled by a dispenser from Gold-Place (model no. MPP-21), was consumed for attaching the IGBT chip to the copper substrate. The preformed bondline that was shaped by stencil printing with Kapton tape was approximately 30 μm thick before sintering.

Five different heating profiles, as presented in Fig. 1 and Table I, were used for chip attachment by nanoscale silver paste. In profile 1, the assembly was directly heated from room temperature (RT) to 275°C at constant heating rate of 7.5°C/min. Profile 2 included three intermediate ramping steps and three dwell stages: room temperature to 50°C at 3°C/min and 20 min dwell time; 50°C to 100°C at 5°C/min and 15 min dwell time; and 100°C to 180°C at 7.5°C/min and 5 min dwell time. These three steps constituted the drying stage. The temperature was eventually increased to 275°C at a rate of 7.5°C/min, and the sample was allowed to soak for 20 min. Compared with profile 2, an extra 10 min at 75°C and a lower heating rate were included in profile 3. For profile 4, the sample was left at room temperature for 1 day before undergoing profile 2. The drying stage of profile 5 was identical to that of profile 2, but in profile 5, static mechanical pressures ranging from 1 MPa to 5 MPa were applied on the surface of the IGBT chip by a hot-press machine provided by CARE Measure & Control, Co., Ltd..[28] The temperature of the hot-press machine was controlled by a T-type thermocouple with precision of ±2°C.

Four printed circuit boards (PCBs) were aluminum wire-bonded to the IGBT chip, and the grid pole, emitter pole, gate pole, and chip thermistor were correspondingly connected to the four PCB plates. At least three samples were prepared for each of the conditions. Finally, the microstructure of each sample was analyzed by optical microscopy and scanning electron microscopy (SEM).

Measurement of IGBT Modules' *K*-Factor

When calculating the transient thermal impedance, the *P–N* junction temperature was needed. Moreover, several electrical properties of the semiconductor, such as the forward voltage of a *P–N* junction and the gate–emitter voltage of the IGBT, were found to be functions of temperature.[29–31] The change of these parameters could be used to infer the junction temperature of the semiconductor die. In this study, with the gride circuit and the gride–emitter voltage of the IGBT chip fixed, the gate–emitter voltage was used as a temperature-sensitive parameter (TSP) to detect the transient thermal impedance.[29,31,32] K is the factor connecting the TSP to the *P–N* junction temperature and could be measured. Figure 2 reveals that the gate–emitter voltage varies linearly with the temperature of the IGBT device as the temperature ranges from 20°C to 100°C. The K-factor could be calculated from the absolute slope of the curve. The value is 9.5 mV/°C in this case, similar to literature values.[29,31,32]

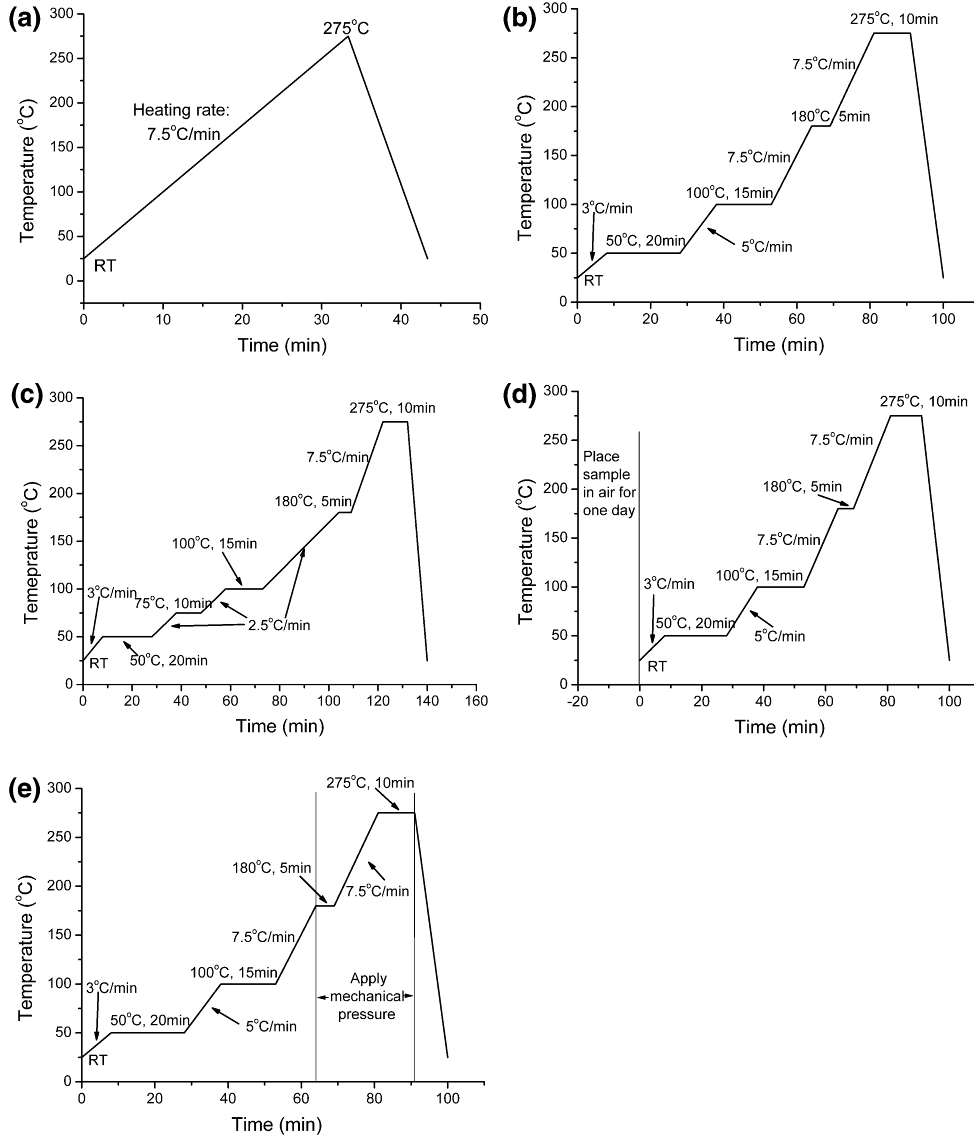

Fig. 1. Sintering profiles used for nanoscale silver-attached IGBT devices: (a) profile 1, (b) profile 2, (c) profile 3, (d) profile 4, and (e) profile 5.

Design of the Transient Thermal Impedance Test System

A system for testing transient thermal impedance was built to verify the bonding quality of the nanoscale silver joints. The system could not only drive the IGBT modules but also maintain a constant heating power. The IGBT module current could be detected by a current induction circuit comprising a switch S_1, resistor R_{s1}, and R_{s2}. The resistance R_{s2} is approximately 1000 times higher than the sum of the on-resistance of S_1 and the resistance R_{s1}. The feedback loop shown in Fig. 3 can be used to regulate the voltage across the sensing network V_s to be equal to $V_{ref}R_2/R_1$ by adjusting V_{ge}. As a result, the grid–emitter voltage could be kept constant.

The waveforms from the thermal impedance measurement are reproduced in Fig. 4. The switch S_1 is turned on during the heating phases $(0 - t_0)$, hence the resistance of the induction circuit is nearly equal to the resistance R_{s1}. Because of the small value of R_{s1}, the grid current $I_{ch} = V_s/R_{s1}$ is large enough to heat up the IGBT modules. The heating power of the IGBT modules is given by Eq. 1:

$$P = I_{ch} \cdot V_{ce} = \frac{V_s \cdot V_{ce}}{R_{s1}}, \qquad (1)$$

where P is the heating power, I_{ch} is the gride current, V_{ce} is the grid–emitter voltage, V_s is the adjustment circuit voltage, and R_{s1} is the resistance.

During the cooling phase $(t_0 - t_1)$, S_1 is turned off. Therefore, the sensing resistance of the network drastically increases from R_{s1} to R_{s2}. Since the voltage reference in the feedback loop does not change, the current flowing through the IGBT is reduced to $I_{cm} = V_s/R_{s2}$. The junction temperature of

Table I. Summary of heating profiles for nanoscale silver sintering

Profile	Procedure	Heating Temperature (°C)	Heating Rate (°C/min)	Holding Time (min)	Pressure (MPa)
1	Step 1	25–275	7.5	N/A	N/A
2	Step 1	25–50	3	N/A	N/A
	Step 2	50	N/A	20	N/A
	Step 3	50–100	5	N/A	N/A
	Step 4	100	N/A	15	N/A
	Step 5	100–180	7.5	N/A	N/A
	Step 6	180	N/A	5	N/A
	Step 7	180–275	7.5	N/A	N/A
	Step 8	275	N/A	10	N/A
3	Step 1	25–50	3	N/A	N/A
	Step 2	50	N/A	20	N/A
	Step 3	50–75	2.5	N/A	N/A
	Step 4	75	N/A	10	N/A
	Step 5	75–100	2.5	N/A	N/A
	Step 6	100	N/A	15	N/A
	Step 7	100–180	2.5	N/A	N/A
	Step 8	180	N/A	5	N/A
	Step 9	180–275	7.5	N/A	N/A
	Step 10	275	N/A	10	N/A
4	Step 1	Placing in air for 1 day at 25°C			
	Step 2	Followed by going through procedure 2			
5	Step 1	25–50	3	N/A	N/A
	Step 2	50	N/A	20	N/A
	Step 3	50–100	5	N/A	N/A
	Step 4	100	N/A	15	N/A
	Step 5	100–180	7.5	N/A	N/A
	Step 6	180	N/A	5	1/3/5
	Step 7	180–275	7.5	N/A	N/A
	Step 8	275	N/A	10	N/A

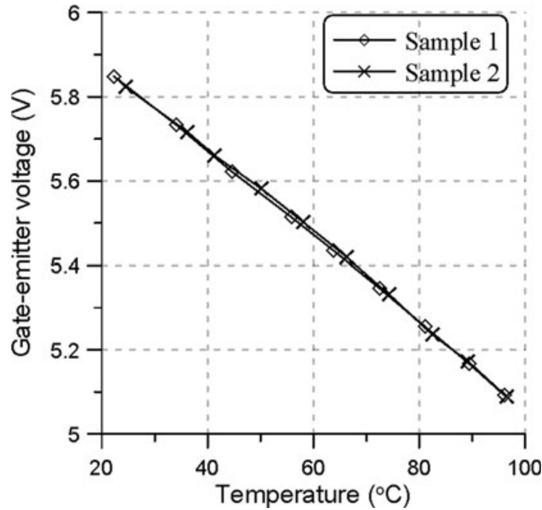

Fig. 2. Relationship between gate–emitter voltage and temperature of IGBT device.

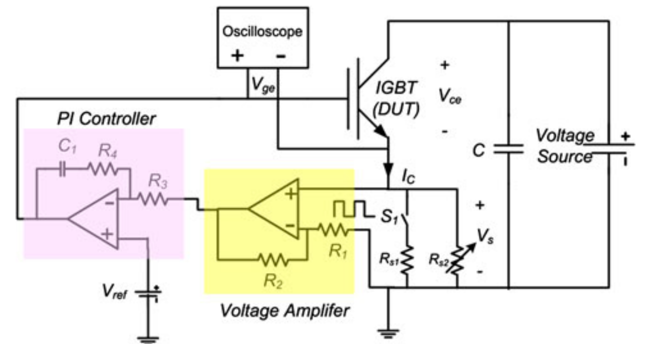

Fig. 3. Schematic diagram of the circuit to generate regulated high-power and low-power pulses for measuring thermal impedance.

the IGBT can then be measured during this period by detecting the variation of V_{ge}. I_{cm} must be large enough to ensure that the device is turned on but not so large as to result in significant self-heating. In the waveform of V_{ge} shown in Fig. 4, V_{ge_i} is the gate voltage before the heating pulse and V_{ge_f} represents the gate voltage after the heating pulse with width of t_h. Thus, the thermal impedance of the sample at time t_h can be calculated as Eq. 2:

$$Z_{th}(t_h) = \frac{V_{ge_i} - V_{ge_f}(t_h)}{K \cdot P}, \quad (2)$$

where Z_{th} is the transient thermal impedance and the value of K is 9.5 mV/°C. The relationship between the transient thermal impedance and the

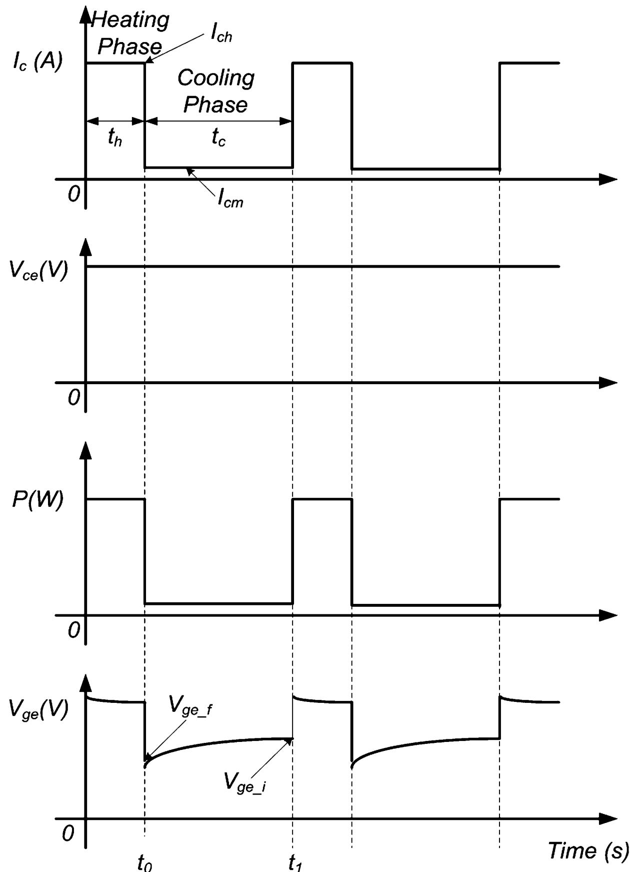

Fig. 4. Waveforms from the thermal impedance measurement.

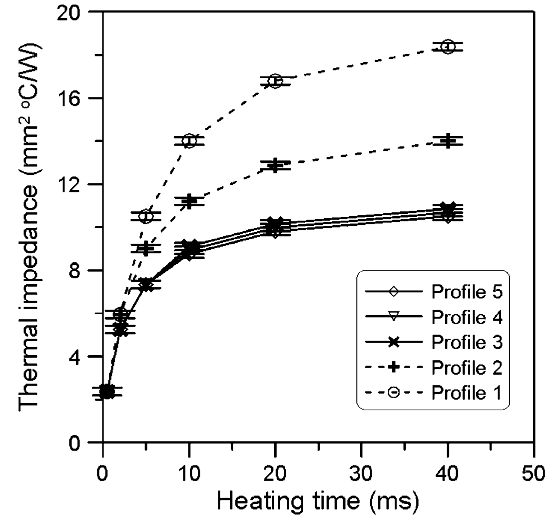

Fig. 5. Thermal impedance of die-attached samples processed by different heating profiles.

heating time t_h can be obtained by changing the width of t_h.

RESULTS AND DISCUSSION

The transient thermal impedances of the samples with nanoscale silver joints sintered using different heating profiles are plotted in Fig. 5. The thermal impedance of samples processed using profile 2 is smaller than those that underwent profile 1, but clearly larger than the samples processed using the other three profiles. On the basis of Gang's work,[22] the thermal impedance consisted mainly of the contributions from the IGBT chip, sintered nanoscale silver joint, and substrate. The thermal impedance of the IGBT chip and copper substrate was constant and would not alter with the sintering conditions, because the thermal conductivities and thicknesses of the chip and substrate were the same for different sintering conditions. Therefore, only the different sintering processes could result in the different thermal impedances of the sintered silver joints. The variation of the measured thermal impedance of the different samples should be attributed to the variation of the thermal impedance of the sintered silver joints due to the different sintering conditions. On this basis and judging from the results of the measurements, we concluded that the thermal impedance of the sintered joints could be reduced by slowing down the heating rate or prolonging the drying time; For example, the thermal impedance of the samples that underwent profile 2 and profile 3 was 23.8% and 41.0%, respectively, being lower than that with profile 1. Since the thermal impedance measured for the samples that underwent profiles 3, 4, and 5, i.e., around 10.5 mm^2·°C/W, are close, we conclude that applying mechanical pressure as low as 1 MPa could lower the thermal impedance to the levels for profiles 3 and 4. Application of external pressure should be a way to reduce the overall processing time without sacrificing the thermal impedance of the joint.

The influence of static pressure on the thermal impedance of the whole assembly is shown in Fig. 6. Higher pressures do not appear to significantly improve the thermal impedance of the assemblies. As far as the thermal impedance is concerned, pressure of 1 MPa is sufficient for achieving low thermal impedance. This conclusion does not necessarily apply to other aspects such as bond strength and reliability, where higher pressures were desirable.[15]

Microstructure analysis was performed by both optical microscopy and SEM to better understand how the different sintering conditions affected the thermal impedance. SEM images of the cross-section of the samples sintered using different heating profiles are shown in Fig. 7. All the samples were processed using profiles that included at least a separate drying stage. Consistent with the measured thermal impedance results, the microstructure of the samples processed under profile 2 had more defects than those of the other samples. The thermal impedance is sensitive to the presence of defects and irregularities in the sintered silver joints.

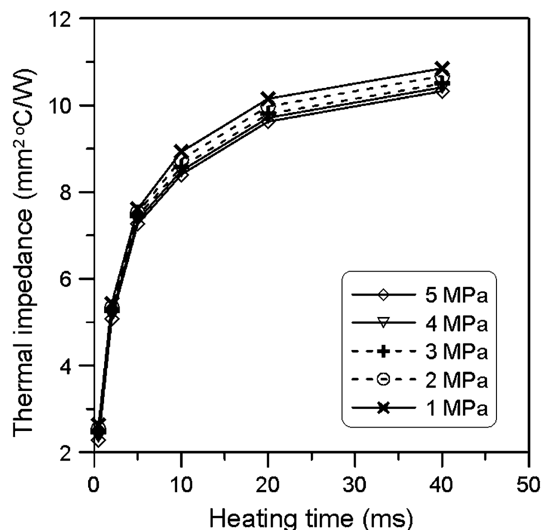

Fig. 6. Thermal impedance of die-attached samples processed by profile 5 under different pressures.

Microstructure images of the samples that were processed under profile 1 and profile 2 are shown in Figs. 8 and 9, respectively. In Fig. 8, the larger joint develops more cracks compared with the smaller joints, because the larger joints suffered from volatilization of solvents or burning out of binders from the nanosilver paste, resulting in more cracks in the joints.[27,33,34] Cracking or delamination in the joint should be reflected in higher impedances. Compared with the samples that underwent profile 1 with die dimensions of 3 mm $\times$ 3 mm and 5 mm $\times$ 5 mm, fewer cracks are also observed along the edge of those that underwent profile 2, as shown in Figs. 8 and 9. Referring to the heating profiles, the main difference lies in the drying stage. Samples processed under profile 1 were not afforded any drying and were heated directly to the sintering temperature. It is highly possible that the cracks developed before the sintering stage so that the structure was worse than that processed under separate drying stages.[33,35,36] Since the nanoscale silver paste

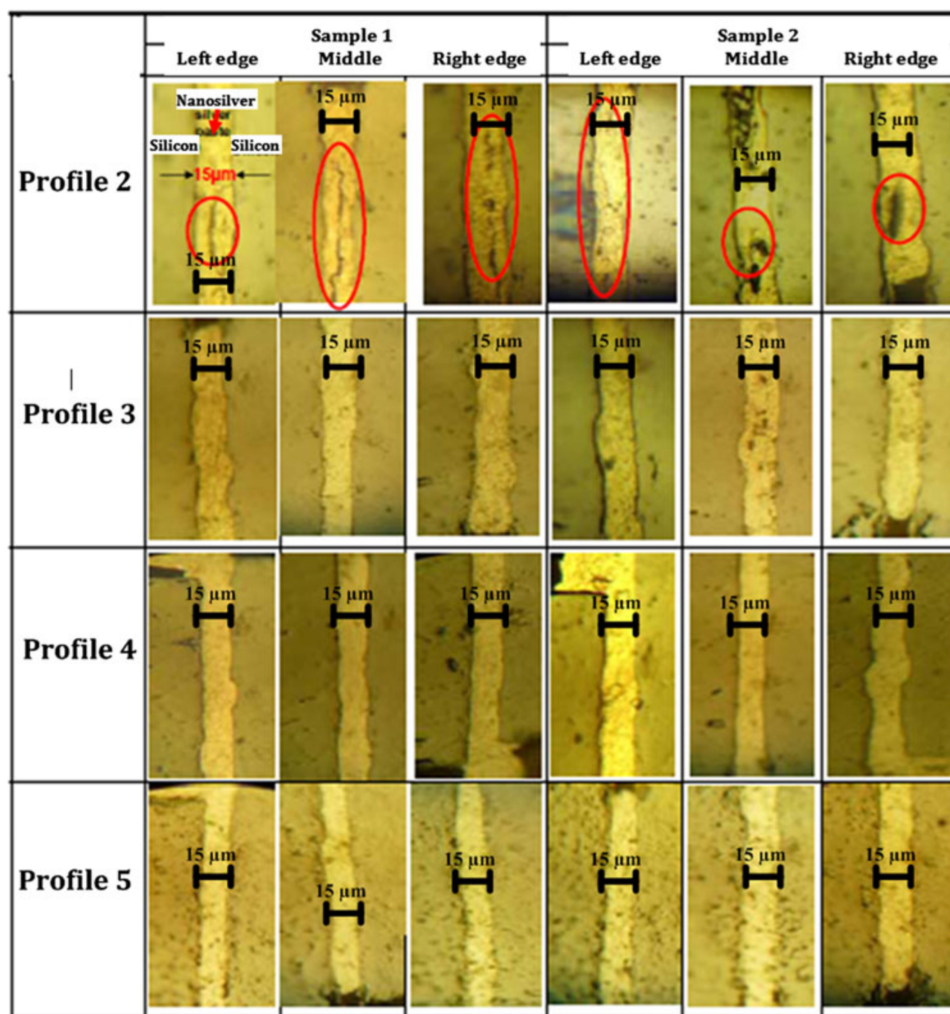

Fig. 7. Cross-sectional microstructures of die-attached samples processed by different heating profiles.

contained a significant amount of solvent, removal of the solvent caused shrinkage in the nanoscale silver layer. The silver layer shrank so fast that the joint had high incidence of defect formation. The cracks along the edges were expected due to large stresses on the periphery of the joint. Therefore, the

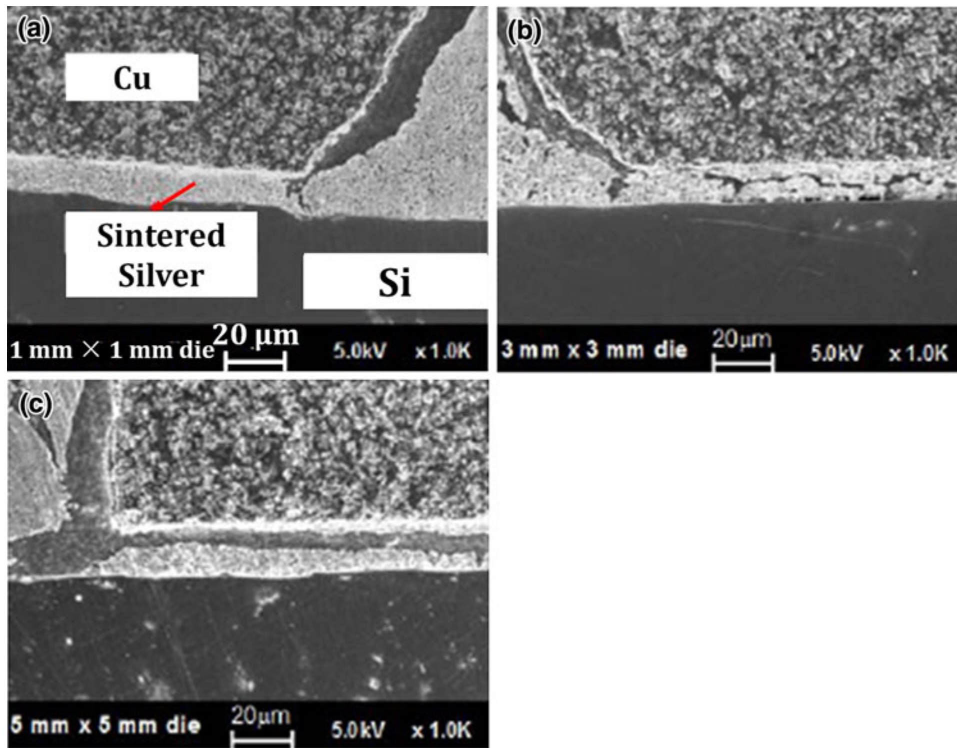

Fig. 8. Cross-sectional SEM images of the die-attach samples that underwent profile 1 with different dimensions: (a) 1 mm × 1 mm, (b) 3 mm × 3 mm, and (c) 5 mm × 5 mm.

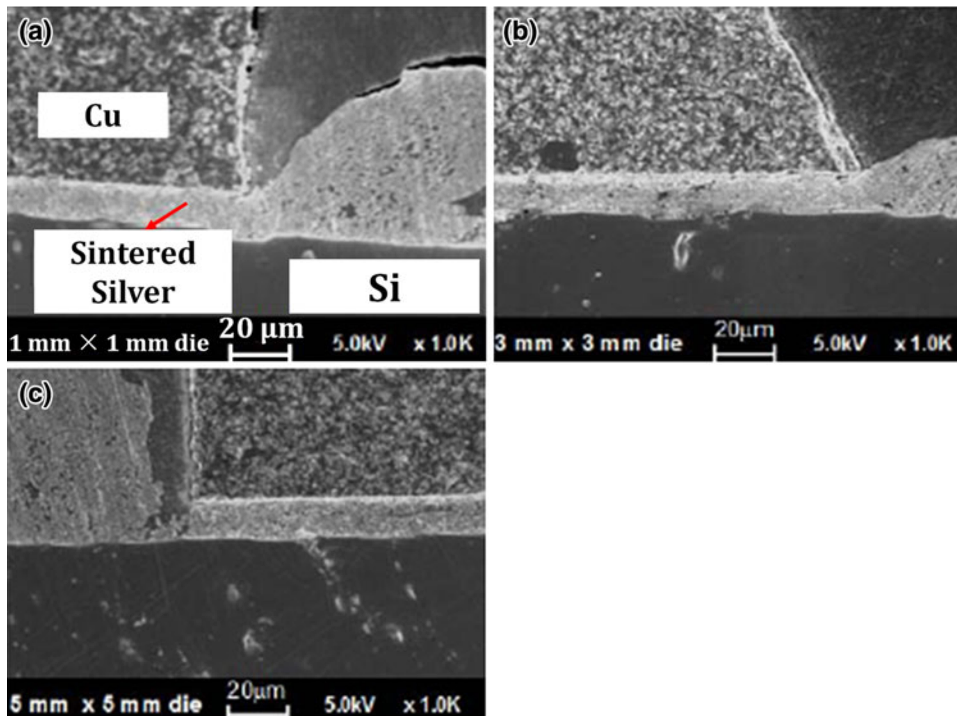

Fig. 9. Cross-sectional SEM images of the die-attach samples that underwent profile 2 with different dimensions: (a) 1 mm × 1 mm, (b) 3 mm × 3 mm, and (c) 5 mm × 5 mm.

thermal impedance of the samples undergoing profile 2 should be lower than that of samples undergoing profile 1, as seen in Fig. 5. In samples processed under profile 2, the microcracks are marked by red ellipses in Fig. 7, being observed at both the interface and the joint. This is similar to what is found in Fig. 9. However, there is no obvious defect in the samples fabricated under profiles 3, 4, and 5, which explains why the thermal impedance of these samples is noticeably low.

On the basis of these observations, we conclude that the defects in the joints were primarily generated by the drying process. Comparison of the samples that underwent profile 2 and profile 5 shows that application of static pressure could prevent the formation of microcracks during drying, hence obtaining sintered silver joints with correspondingly low thermal impedance. Although higher pressure during sintering could improve the density of the silver joint and the bonding strength,[15] the thermal impedance was not affected much as the pressure ranged from 1 MPa to 5 MPa. Transient thermal impedance could be usefully treated as a criterion to evaluate the bonding quality of nanoscale silver joints.

CONCLUSIONS

A Z_{th} measurement method was used to study the transient thermal impedance of assemblies bonded by sintered nanoscale silver. Because the thermal conductivity and thicknesses of the IGBT chip and copper substrate should not be altered by changing the sintering conditions, the variation in the measured thermal impedance of the samples under the different sintering conditions should be only attributed to the sintered silver joint. A correlation was found between the measured thermal impedance and the microstructure of the sintered joints. Joints with defects such as cracks were found to exhibit higher impedance. Based on the measurements, we concluded that the thermal performance of the assemblies could be enhanced by lowering the heating rate during drying, prolonging the drying time, and applying mechanical pressure during sintering. However, exerting pressure beyond 1 MPa during sintering could not significantly improve the thermal performance of sintered silver joints.

Evident cracks were found at the edge of the samples that exhibited high thermal impedance, particularly the samples that underwent profile 1. Slowing down the heating rate during drying and/or exerting mechanical pressure could significantly alleviate microcracking. Pressure of 1 MPa is recommended during the sintering of nanoscale silver joints for large-area die-attachment.

ACKNOWLEDGEMENTS

The authors gratefully acknowledge financial support for this work from the National Natural Science Foundation of China (Nos. 51101112, 10802056, 11172202, 11072171, and 51175375). We would like to acknowledge Dr. Khai Ngo from the Center of Power Electronics Systems in Virginia Tech. In addition, we also want to thank Dr. Jesus Calata and Dr. Thomas G. Lei from Virginia Tech and Ford Motor Company, respectively, for their suggestions.

REFERENCES

1. U. Scheuermann and P. Beckedahl, *CIPS 2008 Proceedings* (2008).
2. E. Schulze, C. Mertens, and A. Lindemann, *PCIM Proceedings* (2009), p. 217.
3. J. Rudzki, C. Mertens, and R. Sittig, *IEEE PESC Proceedings* (2004), p. 4178.
4. G-Q. Lu, G. Lei, and J.N. Calata, U.S. patent 0162557 (2009).
5. Y.H. Mei, G.-Q. Lu, X. Chen, S. Luo, and D. Ibitayo, *IEEE Trans. Device Mater. Reliab.* 11, 2 (2010).
6. Y.H. Mei, G.-Q. Lu, X. Chen, and S.F. Luo, *IEEE Trans. Device Mater. Reliab.* 11, 2 (2010).
7. Y.H. Mei, G.-Q. Lu, X. Chen, C. Gang, S. Luo, and D. Ibitayo, *J. Electron. Mater.* 40, 10 (2011).
8. D.J. Yu, X. Chen, G. Chen, G.-Q. Lu, and Z.Q. Wang, *Mater. Des.* 30, 10 (2009).
9. J.G. Bai, Z.Z. Zhang, J.N. Calata, and G.-Q. Lu, *IEEE Trans. Compon. Packag. Technol.* 29, 3 (2006).
10. J.G. Bai and G.-Q. Lu, *IEEE Trans. Device Mater. Reliab.* 6, 3 (2006).
11. J.N. Calata, T.G. Lei, and G.-Q. Lu, *Int. J. Mater. Prod. Technol.* 34, 94 (2009).
12. G-Q. Lu, J.N. Calata, G. Lei, and X. Chen, *EuroSimE Proceedings* (2007), p. 609.
13. G-Q. Lu, J.N. Calata, and T.G. Lei, *CIPS Proceedings* (2008), p. 121.
14. T. Wang, X. Chen, G.-Q. Lu, and G.-Y. Lei, *J. Electron. Mater.* 36, 10 (2007).
15. T.G. Lei, J.N. Calata, G.-Q. Lu, X. Chen, and S. Luo, *IEEE Trans. Compon. Packag. Technol.* 33, 1 (2010).
16. D. Xu, H. Lu, L. Huang, S. Azuma, M. Kimata, and R. Uchida, *IEEE Trans. Ind. Appl.* 38, 5 (2002).
17. M. Fukuda, *Reliability and Degradation of Semiconductor Lasers and LEDs* (Norwood: Artech House, 1991).
18. T. Yanagisawa, *Microelectron. Reliab.* 38, 10 (1998).
19. T.G. Lei, J. Calata, S.F. Luo, G-Q. Lu, and X. Chen, *Key Eng. Mater.* 353–358 (2007).
20. K. Chu, C. Jia, X. Liang, H. Chen, and H. Guo, *Mater. Des.* 30, 9 (2009).
21. X. Cao, T. Wang, K.D.T. Ngo, and G-Q. Lu, *IEEE Trans. Compon. Packag. Manuf. Technol.* 1, 4 (2011).
22. G. Chen, D. Han, Y.-H. Mei, X. Cao, T. Wang, X. Chen, and G-Q. Lu, *IEEE Trans. Device Mater. Reliab.* 12, 1 (2012).
23. X. Cao, T. Wang, G-Q. Lu, and K. D. T. Ngo, *IPEC Proceedings* (2010), p. 546.
24. L. Xue, P. Keblinski, S.R. Phillpot, S.U.-S. Choi, and J.A. Eastman, *J. Chem. Phys.* 118, 1 (2003).
25. http://www.nbetech.com/. Accessed May 14th, 2012.
26. J.G. Bai, J.N. Calata, and G.-Q. Lu, *IEEE Trans. Electron. Packag. Manuf.* 30, 4 (2007).
27. T. Wang, X. Chen, G.-Q. Lu, and G.-Y. Lei, *J. Electron. Mater.* 36, 10 (2007).
28. www.care-mc.com/. Accessed May 14th, 2012.
29. Z. Jakopovic, Z. Bencic, and F. Kolonic, *ISIE Proceedings* (1999), p. 574.
30. S.M. Sze, *Physics of Semiconductor Devices* (New York: Wiley, 1981).
31. B.J. Baliga, *Fundamentals of Power Semiconductor Devices* (New York: Springer, 2008).

32. J. Zarebski and K. Górecki, *ICIE Proceedings* (1993), p. 111.
33. H. Conrad, Z. Guo, Y. Fahmy, and D. Yang, *J. Electron. Mater.* 28, 9 (1999).
34. X. Li, X. Chen, and G-Q. Lu, *J. Electron. Packag.* 132, 3 (2010).
35. K.-S. Kim, M. Haga, and K. Suganuma, *J. Electron. Mater.* 32, 12 (2003).
36. W. Dong, Y. Shi, Y. Lei, Z. Xia, and F. Guo, *J. Electron. Mater.* 38, 9 (2009).